ELSEVIER

Journal of Power Sources 113 (2003) 151–156

JOURNAL OF POWER SOURCES

www.elsevier.com/locate/jpowsour

Hydrogen absorption studies of an over-stoichiometric zirconium-based AB_2 alloy

W.E. Triaca[a,*], H.A. Peretti[b], H.L. Corso[b], A. Bonesi[a], A. Visintin[a]

[a] *Instituto de Investigaciones Fisicoquímicas Teóricas y Aplicadas, Facultad de Ciencias Exactas, UNLP, Suc. 4, C.C. 16, La Plata 1900, Argentina*

[b] *Centro Atómico Bariloche, CNEA, C.C. 439, San Carlos de Bariloche 8400, Argentina*

Received 9 September 2002; accepted 23 September 2002

Abstract

The hydrogen absorption characteristics and the electrochemical behavior of the $Zr_{0.9}Ti_{0.1}Mn_{0.66}V_{0.46}Ni_{1.1}$ alloy were studied. The pressure–composition isotherms for the alloy show a high hydrogen storage capacity and a steep slope with a slight plateau instead of the horizontal plateau corresponding to the two-phase equilibrium. This feature is attributed to the presence of small amounts of secondary phases due to microsegregation of alloying elements during solidification. The plateau tendency is enhanced upon homogenization annealing of the alloy. The activation of the $Zr_{0.9}Ti_{0.1}Mn_{0.66}V_{0.46}Ni_{1.1}$ alloy electrode in alkaline solution at 30 °C was evaluated by using the cyclic voltammetry technique. For comparison, the $Zr_{0.9}Ti_{0.1}CrNi$ alloy was also studied. The discharge capacities are about 330 mAh/g for both as-melted alloys, but the activation is faster for $Zr_{0.9}Ti_{0.1}Mn_{0.66}V_{0.46}Ni_{1.1}$ than for $Zr_{0.9}Ti_{0.1}CrNi$, indicating that the substitution of Cr by Mn and V enhances the rate of activation due to the formation of metal surface oxides that can be reduced more easily, which increases the reaction surface area. For the annealed $Zr_{0.9}Ti_{0.1}Mn_{0.66}V_{0.46}Ni_{1.1}$ alloy, large charge–discharge overpotentials and a significant decrease in discharge capacity are observed, which is ascribed to the disappearance of catalytic secondary phases present in the as-melted alloy.

Keywords: Metal hydride; Hydrogen absorption; Metal alloy electrode; Battery

1. Introduction

The interest in the study of Zr-based Laves phase metal hydrides, i.e. AB_2-type intermetallic compounds, where A = Zr, Ti and B = Ni, V, Mn, Cr, etc. has increased because their high hydrogen storage capacity is very attractive for battery applications [1]. Several studies have focused on the roles of alloy composition and microstructure in the solid–gas and electrochemical reactions [2–4].

The activation of the alloy plays a key role in the hydrogen absorption process, since it defines the reaction rate of the hydrogen with the metal and the incorporation to its structure. During activation, different processes can occur [5–7], such as: (i) the reduction of metal surface oxides that interfere with hydrogen; (ii) reduction in particle size due to cracks produced by the increase in volume; (iii) changes in the chemical composition and/or surface structure of the metal. It has recently been found that alloy electrodes subjected to periodic potential treatments improve their kinetics properties in comparison with those cycled with the conventional galvanostatic charge–discharge methods [8,9].

In this work, the hydrogen absorption characteristics and the electrochemical properties of as-melted and annealed $Zr_{0.9}Ti_{0.1}Mn_{0.66}V_{0.46}Ni_{1.1}$ alloys are studied in order to determine their possible application as the negative electrode in nickel/metal hydride batteries. For comparison, the characterization of the as-melted $Zr_{0.9}Ti_{0.1}CrNi$ alloy was also carried out. The alloy electrodes were tested along charge and discharge cycles in 7 M KOH at 30 °C, and their discharge capacity and cycle life behavior were evaluated. The effect of applying periodic potential treatments to the alloy electrodes on the activation process was investigated as well.

2. Experimental

The alloy samples were prepared by arc melting adequate proportions of the constituent elements of purity better than

* Corresponding author. Tel.: +54-221-4257291/4257430; fax: +54-221-4254642.
E-mail addresses: wtriaca@inifta.unlp.edu.ar (W.E. Triaca), avisintin@inifta.unlp.edu.ar (A. Visintin).

0378-7753/02/$ – see front matter
PII: S0378-7753(02)00536-0

3N, under a high purity inert atmosphere in a cooled copper hearth. The small button-shaped ingots (≈20 g) were turned over and remelted at least once in order to get good homogeneity. Two alloys of the AB_2-type, of compositions $Zr_{0.9}Ti_{0.1}Mn_{0.66}V_{0.46}Ni_{1.1}$ and $Zr_{0.9}Ti_{0.1}CrNi$, were obtained. Both alloys were used without any further heat treatment, except for the $Zr_{0.9}Ti_{0.1}Mn_{0.66}V_{0.46}Ni_{1.1}$ alloy, a portion of which was wrapped in a Ta foil and annealed at 1000 °C for 10 days inside an evacuated quartz capsule.

The structure and phase morphology of the intermetallic samples were characterized by X-ray diffraction (XRD), scanning electron microscopy (SEM) and energy dispersive spectroscopy (EDS) techniques. The intermetallics were pulverized mechanically and sieved into powders of about 105 mesh for powder diffractometry as well as for electrode preparation.

The pressure–composition–temperature (PCT) curves were measured using a Sieverts-type apparatus. Pieces of about 2 g obtained by crushing the as-melted alloy buttons were loaded into the reactor chamber, brought into vacuum of about 10 Pa and then exposed to a hydrogen atmosphere of 6000 kPa. A pressure drop corresponding to the absorption of a certain amount of hydrogen by the alloy was observed in the closed reactor. After pressure stabilization, desorption was achieved by heating the reactor to 400 °C while evacuating until the base vacuum was restored. After repetition of this absorption–desorption cycle for three times the alloy was considered to be fully activated since the amount of absorbed hydrogen in each cycle no longer increased. Desorption isotherms were then determined at different temperatures by the standard stepwise pressure drop method, after having fully charged the sample at the appropriate temperature.

The preparation of metal alloy powder electrodes requires the use of compacting materials because the active components are brittle and disintegrate upon hydride formation [10]. Thus, working electrodes were prepared by mixing 75 mg of sieved alloy powder (<105 μm) with 75 mg of teflonized carbon (Vulcan XC—72 + 33 wt.% PTFE). The mixed powders were then cold pressed to 3500 kg/cm^2 onto a 1 cm^2 current collector constructed from a porous nickel mesh. The geometric area of the working electrodes was about 2 cm^2. A three-electrode cell with a large surface area counter electrode (sintered NiOOH), containing a 7 M KOH electrolyte at 30 °C was used to determine the electrochemical characteristics of the alloy electrodes. A Hg/HgO electrode was used as reference electrode. To accelerate the activation process, the working electrodes were subjected to sequences of 25 voltammetric cycles at 1 mV/s between −1.4 and −0.4 V. After each sequence of voltammetric cycles, the discharge capacities of the alloy electrodes were monitored by measuring the charge–discharge response of the electrode to constant currents impressed by a battery cycler. In all electrochemical tests, the discharge cut-off potential was −0.6 V versus Hg/HgO reference electrode.

3. Results and discussion

3.1. Structural parameters, XRD and SEM–EDS analysis

The X-ray powder diffraction patterns of the $Zr_{0.9}Ti_{0.1}Mn_{0.66}V_{0.46}Ni_{1.1}$ alloy in the as-melted and annealed conditions using Cu Kα radiation are shown in Fig. 1. From the diffraction angles, the main peaks can be indexed as indicated in the figure, revealing the presence of a major phase with the hexagonal C^{14} ($MgZn_2$-type) structure and lattice parameters: $a = 0.4995 \pm 0.0003$ nm and $c = 0.8155 \pm 0.0005$ nm. These values differ in less than 0.7% from those reported in [1] for an alloy with the same nominal

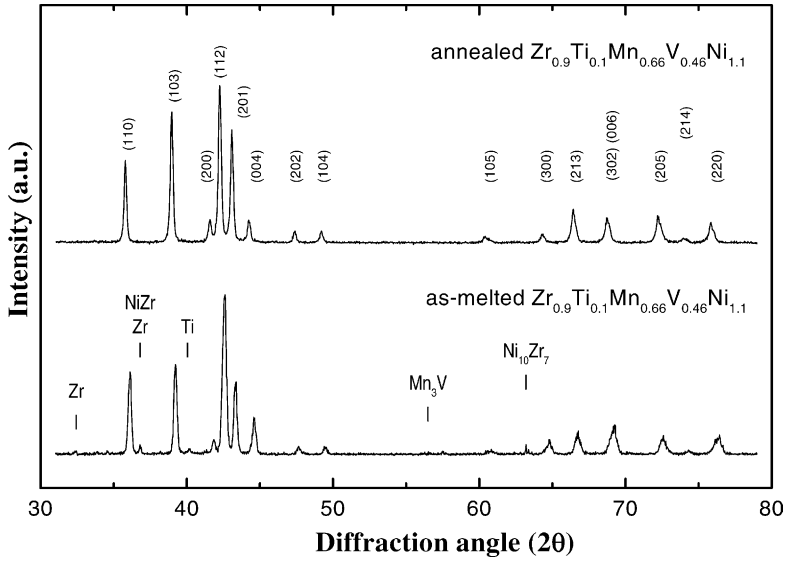

Fig. 1. XRD patterns of $Zr_{0.9}Ti_{0.1}Mn_{0.66}V_{0.46}Ni_{1.1}$ alloy in the as-melted and annealed conditions under Cu Kα radiation.

Table 1
XRD data of small extra peaks in the as-melted $Zr_{0.9}Ti_{0.1}Mn_{0.66}V_{0.46}Ni_{1.1}$ alloy

2θ	Possible phase reflection	Reference [11] card number
32.43	(1 0 0) of Zr	12-0478
36.80	(1 0 1) of Zr and/or (1 1 1) of NiZr	05-0665/12-0478
40.05	(1 0 1) of Ti	44-1294
56.50	(5 1 1) of Mn_3V	07-0389
63.20	(3 5 3) of $Ni_{10}Zr_7$	47-1027

composition and are consistent with the fact that no peaks corresponding to other phases are detected. However, by comparing the diffractograms of the as-melted and annealed samples in detail, the presence of small extra peaks in the as-melted alloy can be observed. This indicates the existence of minor phases formed during solidification that tend to disappear upon heat treatment. An assessment of some possible secondary phases compatible with the extra reflections [11] is indicated in Fig. 1, and with more details in Table 1.

The SEM image of the $Zr_{0.9}Ti_{0.1}Mn_{0.66}V_{0.46}Ni_{1.1}$ alloy in the as-melted condition (Fig. 2a) shows regions of different contrast. Results of EDS microanalysis on clear zones reveal a composition increase of 22% for Zr, 94% for Ti and 48% for Ni with respect to their nominal values, at the expense of a depletion of V and Mn. The resulting atomic proportions of Zr, Ti and Ni within these regions indicate the presence of a compound of approximate composition $Zr_{0.8}Ti_{0.2}Ni$, which would be a variant of the intermetallic compound ZrNi with partial substitution of Zr by Ti, in too

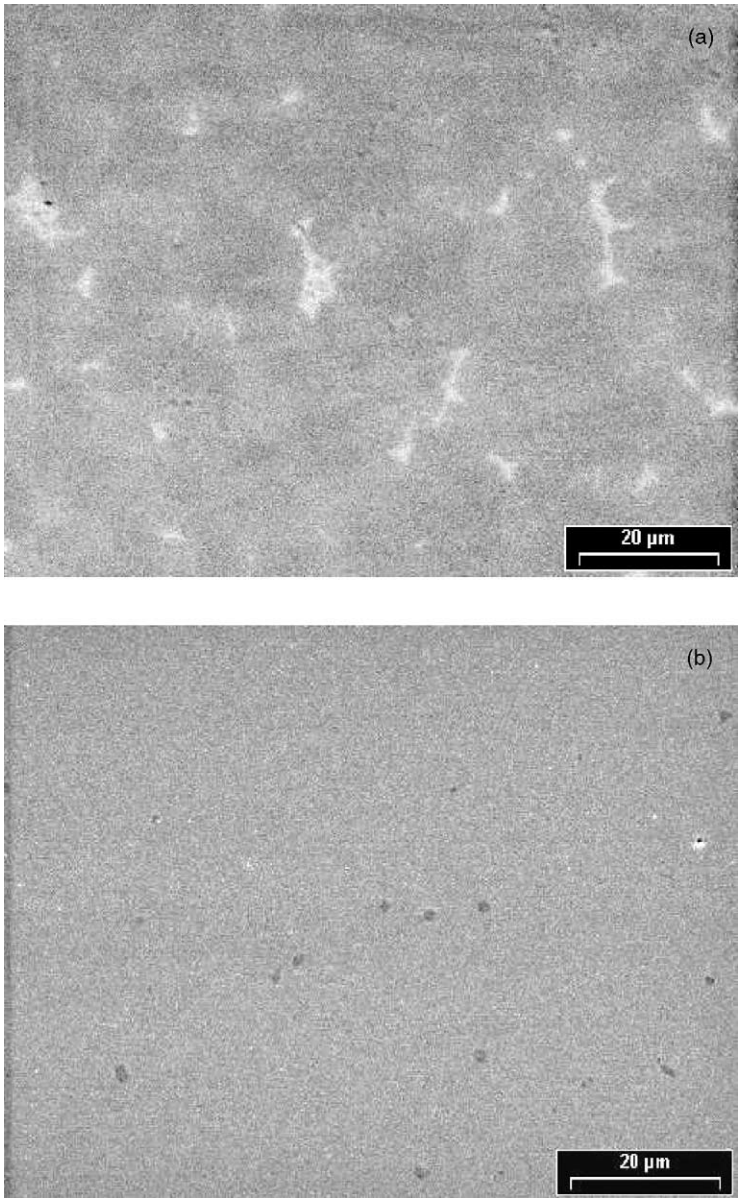

Fig. 2. SEM images of the $Zr_{0.9}Ti_{0.1}Mn_{0.66}V_{0.46}Ni_{1.1}$ alloy: (a) as-melted; (b) annealed.

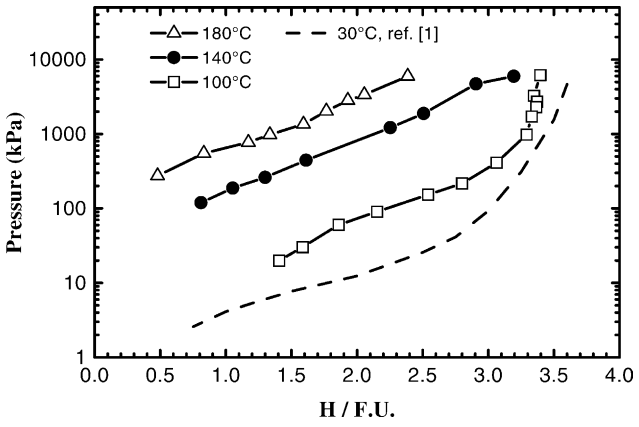

Fig. 3. Pressure–composition desorption isotherms for the as-melted $Zr_{0.9}Ti_{0.1}Mn_{0.66}V_{0.46}Ni_{1.1}$ alloy at different temperatures.

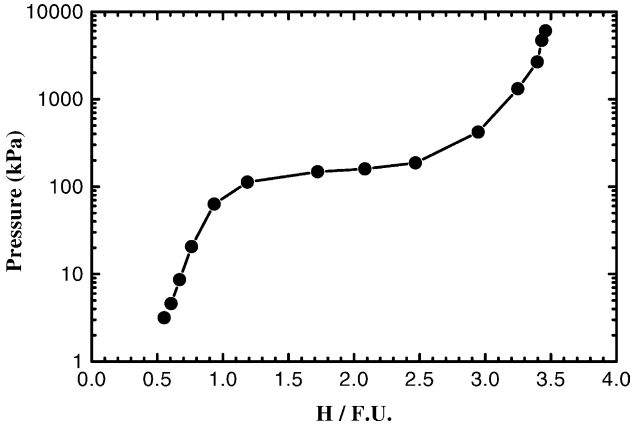

Fig. 4. Pressure–composition desorption isotherm at 100 °C for the annealed $Zr_{0.9}Ti_{0.1}Mn_{0.66}V_{0.46}Ni_{1.1}$ alloy.

small quantities to be clearly detected by X-rays. In the rest of the microstructure (grey zone), the detected composition is consistent with nominal values. These results confirm the microsegregation of alloying elements during solidification, which is usually observed in alloys without any further thermal homogenization treatment. This effect is more likely to be expected for alloys with a higher number of alloying elements and undergoing rapid solidification. These are just the conditions given in this work as well as in [1], where an electric arc furnace was employed to melt the alloys. A similar microsegregation effect was observed in the $Zr_{0.9}Ti_{0.1}CrNi$ alloy without heat treatment, as reported in [8].

On the other hand, the SEM image and EDS microanalysis of the annealed $Zr_{0.9}Ti_{0.1}Mn_{0.66}V_{0.46}Ni_{1.1}$ alloy reveal a single homogeneous phase in accordance with its nominal composition, except for some minor segregation of pure Zr, revealed as small round darker zones (Fig. 2b).

From the above described results, it becomes clear that in the as-melted alloy there is a certain degree of microsegregation of alloying elements. This gives rise to a variation in the alloy composition and the formation of small amounts of secondary phases that are not present in the annealed alloy where a better homogenization of its composition is achieved.

3.2. Pressure–composition isotherms

The PCT curves for the as-melted $Zr_{0.9}Ti_{0.1}Mn_{0.66}V_{0.46}Ni_{1.1}$ alloy obtained at 100, 140 and 180 °C are shown in Fig. 3. As can be seen, the measured isotherms present a steep slope with a slight plateau tendency similar to that reported in [1] for the same alloy at 30 °C. This feature is attributed to the presence of minor phases formed during solidification. Saturation for the isotherm at 100 °C occurs at hydrogen pressures above 2000 kPa for a value of about 3.4 hydrogen atoms per formula unit (H/F.U.), whereas at 500 kPa the H/F.U. ratio is 3.2. Otherwise, the annealing treatment of the alloy leads to a flattening of the steep slope of the PCT curves, as shown in Fig. 4 for the desorption isotherm at 100 °C since, as expected, the secondary phases tend to disappear with heat treatment [12].

3.3. Electrochemical data

The activation process of the AB_2-type alloy electrodes for the hydrogen absorption in a KOH solution at 30 °C was studied by using the cyclic voltammetry technique. This procedure has been found to be effective in accelerating the activation process [9,13]. Charge–discharge cycles run for the as-melted $Zr_{0.9}Ti_{0.1}Mn_{0.66}V_{0.46}Ni_{1.1}$ and $Zr_{0.9}Ti_{0.1}CrNi$ alloy electrodes after application of cyclic voltammetric seans at 1 mV/s between −1.4 and −0.4 V are shown in Fig. 5. The $Zr_{0.9}Ti_{0.1}Mn_{0.66}V_{0.46}Ni_{1.1}$ alloy exhibits lower overpotentials and a higher discharge capacity than the $Zr_{0.9}Ti_{0.1}CrNi$ alloy. On the other hand,

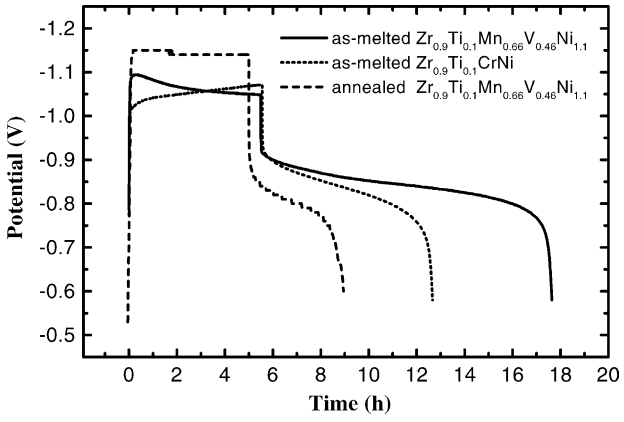

Fig. 5. Charge–discharge cycles at constant current after 25 voltammetric cycles for the $Zr_{0.9}Ti_{0.1}Mn_{0.66}V_{0.46}Ni_{1.1}$ alloy in the as-melted and annealed conditions and after 50 voltammetric cycles for the as-melted $Zr_{0.9}Ti_{0.1}CrNi$ alloy. *I* (charge): 6 mA; *I* (discharge): 2 mA; 7 M KOH; 30 °C.

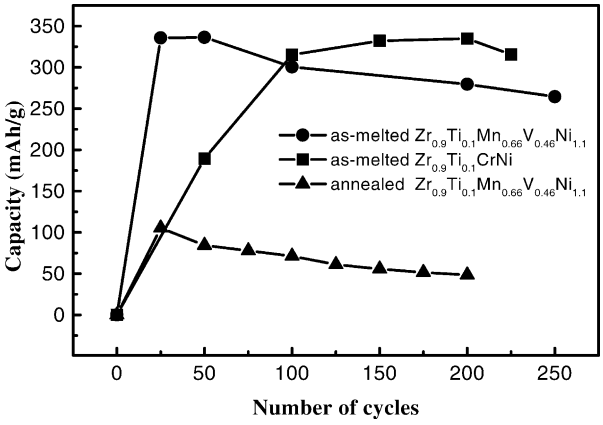

Fig. 6. Discharge capacity vs. number of voltammetric cycles at 1 mV/s for different alloys. Lower and upper potential limits: −1.4 and −0.4 V; 7 M KOH; 30 °C.

the annealing treatment of the $Zr_{0.9}Ti_{0.1}Mn_{0.66}V_{0.46}Ni_{1.1}$ alloy produces an increase in charge–discharge overpotentials and a significant decrease in discharge capacity (Fig. 5).

The as-melted $Zr_{0.9}Ti_{0.1}Mn_{0.66}V_{0.46}Ni_{1.1}$ alloy reaches its maximum capacity after 25 voltammetric cycles, whereas the as-melted $Zr_{0.9}Ti_{0.1}CrNi$ alloy requires 175 cycles (Fig. 6). Under these conditions, charge storage capacities of 324 mAh/g for the $Zr_{0.9}Ti_{0.1}Mn_{0.66}V_{0.46}Ni_{1.1}$ alloy and 330 mAh/g for the $Zr_{0.9}Ti_{0.1}CrNi$ alloy were obtained. For the annealed $Zr_{0.9}Ti_{0.1}Mn_{0.66}V_{0.46}Ni_{1.1}$ alloy, the capacity attains a maximum value of only 100 mAh/g after 25 voltammetric cycles (Fig. 6).

The faster activation of the $Zr_{0.9}Ti_{0.1}Mn_{0.66}V_{0.46}Ni_{1.1}$ alloy with respect to that of the $Zr_{0.9}Ti_{0.1}CrNi$ alloy indicates that the substitution of Cr by Mn and V leads to an acceleration of the activation process, probably due to the formation of metal surface oxides that can be reduced more easily, increasing the reaction surface area.

Otherwise, the large charge–discharge overpotentials and the significant reduction in discharge capacity of the annealed $Zr_{0.9}Ti_{0.1}Mn_{0.66}V_{0.46}Ni_{1.1}$ alloy should be attributed mainly to the resulting phase homogenization due to the annealing treatment, which leads to the disappearance of microsegregated catalytic phases rich in Ni that improve the kinetics of hydrogen absorption–desorption processes [12,14,15]. In addition, the presence of pure Zr in the annealed sample may lead to the formation of oxide barriers, e.g. ZrO_2, which prevents the difussion of hydrogen within the bulk of the alloy [15].

The fact that the measured discharge capacity of the as-melted $Zr_{0.9}Ti_{0.1}Mn_{0.66}V_{0.46}Ni_{1.1}$ alloy is slightly smaller than that of the alloy with the same nominal composition (392 mAh/g) reported in [1], can be ascribed to small differences in the composition of the alloy, since its behavior is very sensitive to small variations in alloying element contents. This is in agreement with the small differences found in the corresponding lattice parameters.

4. Conclusions

The XRD analysis reveals a hexagonal structure for the $Zr_{0.9}Ti_{0.1}Mn_{0.66}V_{0.46}Ni_{1.1}$ alloy. SEM–EDS measurements of the alloy in the as-melted condition indicate some compositional variations in the microstructure, typical of solidified alloys without any further thermal homogenization treatment. The pressure–composition isotherms for the as-melted alloy exhibit a high hydrogen storage capacity and a steep slope with a slight plateau tendency that can be ascribed to the presence of small amounts of secondary phases due to microsegregation of alloying elements during solidification. On the other hand, the annealed alloy presents an enhanced plateau in agreement with a more homogeneous composition, as revealed by SEM–EDS experiments.

The electrochemical results show that the as-melted $Zr_{0.9}Ti_{0.1}Mn_{0.66}V_{0.46}Ni_{1.1}$ and $Zr_{0.9}Ti_{0.1}CrNi$ alloys present high charge storage capacity values practically of the same order. However, the activation of the former is achieved faster, indicating that the substitution of Cr by Mn and V leads to an acceleration of the activation process, probably due to the formation of metal surface oxides that can be reduced more easily, which increases the reaction surface area.

The increase in charge–discharge overpotentials and the decrease in discharge capacity of the $Zr_{0.9}Ti_{0.1}Mn_{0.66}V_{0.46}Ni_{1.1}$ alloy after the annealing treatment should be attributed to the disappearance of minor phases rich in Ni that are present in the as-melted alloy. These secondary phases exhibit a high catalytic activity for the electrochemical charge–discharge processes.

Acknowledgements

This work was supported by the Agencia Nacional de Promoción Científica y Tecnológica of Argentina, the Consejo Nacional de Investigaciones Científicas y Técnicas, the Comisión de Investigaciones Científicas de la Provincia de Buenos Aires and the Cooperativa de Electricidad Bariloche.

References

[1] D.M. Kim, S.W. Jeon, J.Y. Lee, J. Alloys Compd. 279 (1998) 209.
[2] J.M. Joubert, M. Latroche, A. Percheron-Guégan, J. Bouet, J. Alloys Compd. 240 (1996) 219.
[3] E. Boschung, A. Züttel, D. Chartouni, L. Schlapbach, J. Alloys Compd. 274 (1998) 294.
[4] M. Bououdina, H. Enoki, E. Akiba, J. Alloys Compd. 281 (1998) 290.
[5] A. Anani, A. Visintin, K. Petrov, S. Srinivasan, J. Reilly, J. Johnson, R. Schwarz, P. Desch, J. Power Sources 47 (1994) 261.
[6] M.V.C. Sastri, B. Viswanathan, S. Srinivasa Murthy, Metal Hydrides. Fundamentals and Applications, Springer, Berlin, 1998.

[7] D.M. Kim, S.M. Lee, K.J. Jang, J.Y. Lee, J. Alloys Compd. 268 (1998) 241.
[8] A. Visintin, H.A. Peretti, C.A. Tori, W.E. Triaca, Int. J. Hydrogen Energy 26 (2001) 683.
[9] H.A. Peretti, A. Visintin, H.L. Corso, A.R. Bonesi, W.E. Triaca, Latin Am. Appl. Res. 32 (2002) 299.
[10] K. Petrov, A. Rostami, A. Visintin, S. Srinivasan, J. Electrochem. Soc. 141 (1994) 1747.
[11] JCPDS-International Centre for Diffraction Data, 1997.
[12] B. Klein, N. Simon, S. Klyamkine, M. Latroche, A. Percheron-Guégan, J. Alloys Compd. 280 (1998) 284.
[13] A. Visintin, H.A. Peretti, C.A. Tori, J.C. Bolcich, W.E. Triaca, Hydrogen Energy Progr. XII 2 (1998) 1193.
[14] W.K. Zhang, C.A. Ma, X.G. Yang, Y.Q. Lei, Q.D. Wang, G.L. Lu, J. Alloys Compd. 293 (1999) 691.
[15] M. Bououdina, C. Lenain, L. Aymard, J.L. Soubeyroux, D. Fruchart, J. Alloys Compd. 27 (2001) 178.